Polymer 50 (2009) 5276–5287

Contents lists available at ScienceDirect

Polymer

journal homepage: www.elsevier.com/locate/polymer

Self-Assembly structures through competitive interactions of miscible crystalline–amorphous diblock copolymer/homopolymer blends

I-Hong Lin [a], Shiao-Wei Kuo [b,**], Feng-Chih Chang [a,*]

[a] Institute of Applied Chemistry, National Chiao Tung University, Hsin Chu, Taiwan
[b] Department of Materials and Optoelectronic Science, Center for Nanoscience and Nanotechnology, National Sun Yat-Sen University, Kaohsiung, Taiwan

ARTICLE INFO

Article history:
Received 4 May 2009
Received in revised form
9 July 2009
Accepted 4 September 2009
Available online 13 September 2009

Keywords:
Self-assembly
Block copolymer
Hydrogen bonding

ABSTRACT

A series of miscible crystalline–amorphous diblock copolymers, (poly(ε-caprolactone)-*b*-(vinyl phenol), PCL-*b*-PVPh) were prepared through sequential ring-opening and controlled living free radical (nitroxide-mediated) polymerizations and then blended with poly(vinyl pyrrolidone) (PVP) homopolymer. Specific interactions, miscibility, and self-assembly morphologies mediated by hydrogen bonding interactions of this new A-B/C type blend, were investigated in detail. Micro-phase separation of these miscible PCL-*b*-PVPh diblock copolymers occurs by blending with PVP through competitive hydrogen bonding interaction in this A-B/C blend. FTIR, XRD, and DSC analyses provide positive evidences that the carbonyl group of PVP is a significantly stronger hydrogen bond acceptor than PCL, thus the PCL block is excluded from the PVPh/PVP miscible phase to form self-assembly structure. ^{13}C CP/MAS solid-state NMR spectra provide additional evidence confirming that micro-phase separation occurs in the blend system because of the presence of more than two $T_{1\rho}(H)$ values for this A-B/C blend system. According to the result of the FTIR and SAXS results, the smaller molecular weight system contains a greater fraction of the hydrogen-bonded carbonyl group, cause indirectly the high degree of phase separation among these blends. In addition, the SAXS profiles possess a sharp primary peak and highly long range ordered reflections q/q^* ratios of 1:2:3 at lower PVP content, an indication of the lamellar structure in the blend which is consistent with TEM image. The phase behavior and morphology shifts from lamellar to cylinder structure with further increase in the PVP content.

1. Introduction

Polymer blends of diblock (A-*b*-B) copolymers with homopolymers have attracted great interest in polymer science recently because of their unusual phase behavior [1–26]. Most prior studies have concentrated on an immiscible A-*b*-B diblock copolymer blended with a homopolymer A [1–3]. Other systems have also been investigated involving blends of an immiscible A-*b*-B diblock copolymer and a homopolymer C, where C is immiscible with block A but interacts favorably with block B [7–13]. In addition, blend systems comprising an immiscible A-*b*-B diblock copolymer and a homopolymer C where homopolymer C is miscible with both A and B have been investigated. For instance, Zhao et al. [8] studied blends of poly(styrene-*b*-vinyl phenol)/poly(vinyl methyl ether) (PS-*b*-PVPh/PVME) where PVME is miscible with both PS and PVPh blocks serving as a common solvent and results in a single phase when the PVME content is higher than 50 wt%. Guo et al. [13,14] reported an immiscible A-*b*-B diblock copolymer, where C is miscible with both blocks A and B, but the hydrogen bonding interactions between the B and C segments is stronger than those of the A and C segments ($\chi_{BC} >> \chi_{AC}$). The selective hydrogen bonding interaction leads to the formation of a variety of composition-dependent microphase separations. These A and B segments in A-*b*-B block copolymers from previous studies are essentially all immiscible. Therefore, our motivation is to exploit the possible self-assembly nanostructure within the A-*b*-B/C blend system where A and B segments are miscible.

Most synthetic polymers are inherently flexible and long-chain nature, specific interactions in polymer blends usually result in an uncontrollable way and lead to formation of irregular structures [27]. Therefore, it is a great challenge to construct regular self-assembly structures through specific interactions from polymeric building blocks in bulk state. When all three binary pairs (B/A, B/C, and A/C) are miscible in a (A/B/C) ternary blend system, a closed immiscibility loop phase separation diagram has been observed [28]. This phenomenon is caused by the difference in the interaction energies among these binary systems, "$\Delta\chi$" and "ΔK" effects in

* Corresponding author. Tel./fax: +886 3 5131512.
** Corresponding author. Fax: +886 7 5254099.
E-mail addresses: kuosw@faculty.nsysu.edu.tw (S.-W. Kuo), changfc@mail.nctu.edu.tw (F.-C. Chang).

0032-3861/$ – see front matter © 2009 Elsevier Ltd. All rights reserved.
doi:10.1016/j.polymer.2009.09.012

ternary polymer blends as described in PVPh/PVAc/PEO [29], SAA/PMMA/PEO [30], and phenolic/PEO/PCL [31] systems. Nonetheless, regular self-assembly structures have rarely been observed. In this study, a miscible diblock copolymer was blended with a homopolymer tending to confine the phase separation at nanometer scale.

In our previous studies [32,33], we first reported a A-*b*-B/C system, poly(vinyl phenol-*b*-methyl methacrylate)/poly(vinyl pyrrolidone) (PVPh-*b*-PMMA)/PVP, where interaction parameters of χ_{AB}, χ_{BC}, and χ_{AC} are all negative but in different values (all binary blends are miscible). In other words, PVPh-*b*-PMMA block (A-*b*-B) copolymer, PVPh/PVP (A/C), and PMMA/PVP (B/C) blends are all miscible through hydrogen bonding interaction or dipole-dipole interaction. However, the hydrogen bonding interaction between PVPh (A) and PVP (C) segments is significantly stronger than that between PVPh (A) and PMMA (B) segments. As a result, this originally miscible PVPh-*b*-PMMA copolymer becomes immiscible by incorporation with 20 ~ 60 wt% PVP and self-assembly morphologies are formed due to significant difference in hydrogen bond interaction strength. In this case, the phase separated PMMA domain can be determined by two T_gs phenomenon based on differential scanning calorimetry (DSC) analyses. All these three segments in our previous studies are amorphous homopolymers, however, in a crystalline–amorphous (C–A) diblock copolymer, the formation of specific structure becomes more complicated as the crystallization driving force perturbs the melt mesophase formed by microphase separation [34].

In this study, we turn our attention to a blend system composed of a miscible crystalline–amorphous diblock copolymer (poly(ε-caprolactone)-*b*-(vinyl phenol)), (PCL-*b*-PVPh) and PVP. The PCL crystallization is expected to undergo more drastic morphological perturbation as compared with previous amorphous PVPh-*b*-PMMA/PVP blend system [32,33]. PCL is a highly crystalline polymer miscible with several amorphous polymers through specific interactions that has been discussed in previous study [35]. In our previous studies [36–40], we also studied blends of PCL with various amorphous hydrogen bonding donating polymers, such as poly(vinyl phenol) (PVPh), phenolic resin, and phenoxy resin. However, the blend of crystalline–amorphous diblock copolymer with other homopolymers through hydrogen bonding interaction has rarely been reported based on our knowledge. PVPh possessing"proton-donor"groups has been reported to form miscible blends with several polymers containing accessible"proton-acceptor"groups, such as acrylate, ester, ether, pyridine, and hydroxyl groups through hydrogen bonding interaction [41–44]. Based on the Painter–Coleman association model (PCAM) [45], the inter-association equilibrium constant ($K_A = 90$) [36] between the carbonyl group of PCL and the hydroxyl group of PVPh is significantly weaker than the inter-association equilibrium constant ($K_A = 6000$) [46] between the carbonyl amide group of PVP and the hydroxyl group of PVPh. In other words, the hydrogen bonding interaction between PVPh and PVP is expected to dominate over that between PVPh and PCL in this PVPh-*b*-PCL/PVP blend. As a result, the PCL block tends to be excluded from the PVPh/PVP mixed rich phase and forms its own domains with regular self-assembly structure.

Herein, a series of PVPh-*b*-PCL diblock copolymers were synthesized through combination of two different living polymerizations (ring-opening and nitroxide-mediated polymerizations in sequential) and then converted to PCL-*b*-PVPh block copolymers through base-catalyzed hydrolysis. Furthermore, the specific interactions and diversity of phase behaviors within these PVPh-*b*-PCL/PVP blends were investigated through differential scanning calorimetry (DSC), one and two-dimensional Fourier transform infrared (FTIR) spectroscopies, high-resolution solid-state ^{13}C CP/MAS NMR spectroscopy, small angle X-ray Scattering (SAXS), and transmission electron microscopy (TEM) analyses.

2. Experimental section

2.1. Materials

All solvents, monomers, and 2,2,6,6-tetramethyl-1-piperidinyloxy (TEMPO) (Aldrich) were vacuum distilled immediately prior to use. 4-Acetoxystyrene (AS) was purified by column chromatography and the ε-caprolactone (ε-CL) was distilled from calcium hydride before use. Styrene was stirred over CaH_2 overnight and distilled under vacuum. All these purified monomers were stored in a freezer and all solvents were distilled prior to use. Triethyaluminum (0.1 mol/L), from TCI was employed as catalysts. Benzoyl peroxide (Acros) was recrystallized from chloroform–methanol (1:1) mixture. 2,2,6,6-tetramethyl-1-piperidinyloxy (TEMPO) and sodium hydroxide were laboratory grade (Wako) and used as received. PVP (weight-average molecular weight: ca. 11000 g/mol and 58000g/mol) was obtained from Scientific Polymer Products.

2.2. Synthesis of 1-hydroxy-2-phenyl-2-(2′,2′,6′,6′-tetramethyl-1-piperidinyloxy) ethane (TEMPO-OH)

Benzyl peroxide (4.0 g, 12.4 mmol) and 160 mL distilled styrene were placed in dry flask, then 2,2,6,6-tetramethyl-1-piperidinyloxy (TEMPO) (5.68 g, 36.4 mmol) was added into the flask with constant stirring at 80 °C under an argon atmosphere. After 24 h, the solution was cooled and freeze-pump-thaw cycles were used to remove residual solvent. Precursor (3.2 g, 8.4 mmol) and 100 mL ethanol were placed in a dry flask; 10 mL of 1 N NaOH solution was added to the flask with a magnetic stirring bar and the mixture was heated to reflux under a nitrogen atmosphere. The combined organic layers were dried with magnesium sulfate and evaporated to dryness. The crude product was purified by flash chromatography eluting with 1:4 hexane/dichloromethane and the content of dichloromethane was gradually increasing to 1:9, then the hydroxyl derivative was obtained.

2.3. Preparation of the prepolymer of polycaprolactone (PCL-TEMPO)

The TEMPO-OH (0.0728 g, 2.5×10^{-4} mol) dissolved in toluene (5 mL) was added into 0.2 mL of a toluene solution of triethyaluminum (0.1 mol/L) under an argon atmosphere. The reaction mixture was stirred at room temperature for 30 min, then evaporated to dryness and removed the byproduct, 2-propanol. After repeating this procedure several times, 5 mL caprolactone (0.044 mol) dissolved in 25 mL dry toluene was added to the reaction mixture in ice bath. The polymerization was carried out at 25 °C for a given time under an argon atmosphere and terminated by adding excess acetic acid (0.2 mL acetic acid/0.8 ml toluene). Two-thirds of the initial solvent was evaporated, and the residue was precipitated into methanol. The product was dried until constant weight under vacuum. The conversion of the polymerization was determined by ^1H NMR.

2.4. Preparation of the PCL-b-PAS diblock copolymer

The prepolymer, PCL-TEMPO, was added into a dry glass tube containing the acetoxystyrene monomer. Twice freeze-pump-thaw cycles were preformed to remove residual solvent. The tube was sealed under vacuum and placed in an oil bath maintained at 120 °C. After 24 h reaction time, the polymerization was terminated by cooling the tube using ice water. After being dissolved in THF, the copolymer was precipitated in methanol and dried in an oven at 50 °C for 24 h to obtain a white powder. The conversion of the polymerization was determined by ^1H NMR.

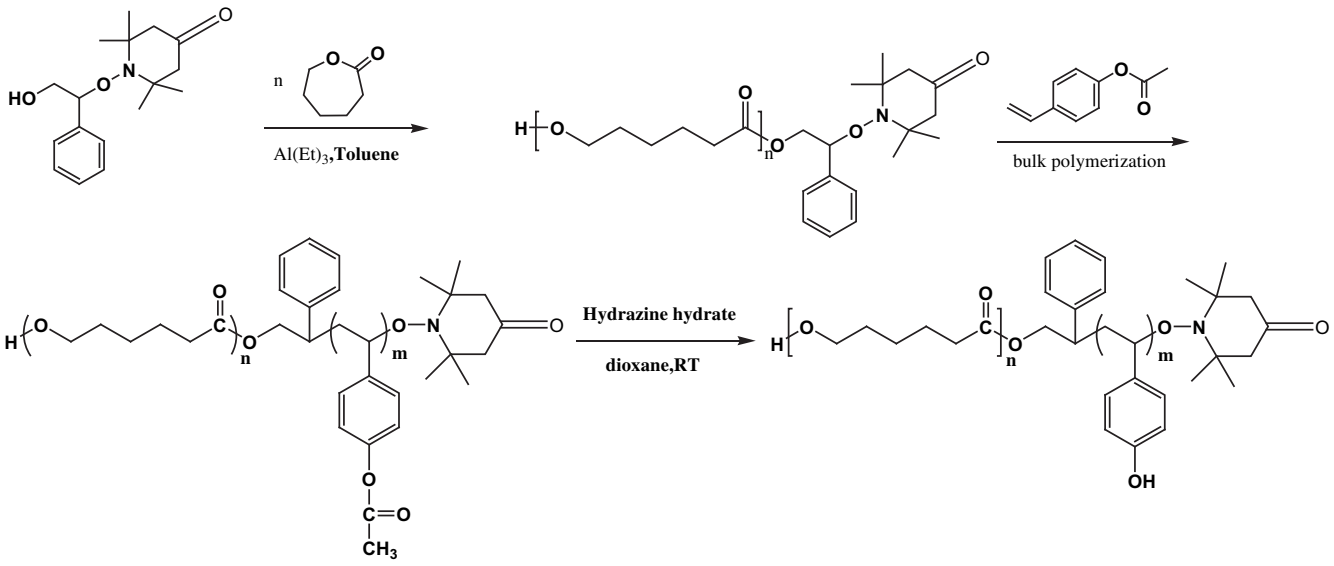

Scheme 1. Synthesis of PCL-*b*-PVPh block copolymers.

2.5. Selective hydrolysis of PCL-b-PAS diblock copolymer

The PCL-*b*-PVPh was prepared from the selective hydrolysis of the PAS block of the PCL-*b*-PAS copolymer. Removal of the acetyl protecting groups from the PAS was carried out by treating with hydrazine hydrate in 1,4-dioxane at room temperature. Typically, the PCL-*b*-PAS (7.2 mmol of AS) copolymer was dissolved in 1,4-dioxane (30 mL) placed in a flask, then hydrazine hydrate (3 mL) was added via a syringe (the volume ratio of hydrazine hydrate to 1,4-dioxane was 1:9). The reaction was maintained at room temperature under an argon atmosphere for 10 h. The solution was concentrated by evaporation of the solvent, washed with deionized water several times, and then dried in a vacuum oven at room temperature for 72 h. Scheme 1 illustrates all these synthesis strategies of the preparation of PVPh-*b*-PCL diblock copolymer.

2.6. Blend preparation

Various PVPh-*b*-PCL/PVP blends with desired compositions were dissolved in *N*,*N*-dimethylformamide to form 5 wt% polymer solutions. The solution was stirred for 24 h, cast onto a Teflon dish, and most of the solvent was evaporated at 100 °C for 24 h. The blend was then dried at 150 °C for additional 7 days for the removal of the residual solvent. To eliminate solvent effect on PCL crystallization, all bulk samples were annealed at 250 °C for 10 min, because the temperature is higher than the glass transition temperature (T_g) of the PVPh block ($T_g^{PVPh} = 180$ °C) and the equilibrium melting point ($T_m^0 = 69$ °C) of the PCL block.

2.7. Characterizations

Thermal analysis was performed using a differential scanning calorimeter (DSC) from TA instrument, Q-20, calibrated by indium. The measurement was operated at a cooling rate of 5 °C/min from 250 °C to −90 °C with sample weight of 5–10 mg. Infrared spectroscopy was recorded on a Nicolet Avatar 320 FTIR spectrophotometer, and 32 scans were collected with a spectral resolution of 1 cm^{-1}. Infrared spectra of these polymer blends were determined through the conventional NaCl disk method. The film used in this study was sufficiently thin to obey the Beer–Lambert law. The 2D correlation analysis was performed using the 2D Shige software composed by Shigeaki Morita (Kwansei-Gakuin University, Japan). In the 2D correlation maps, the white regions are defined as the positive correlation intensities, whereas the shaded ones are regarded as the negative correlation intensities [47,48]. Molecular weight and molecular weight distribution were determined through gel permeation chromatography (GPC) using a Waters 510 HPLC equipped with a 410 differential refractometer, a refractive index (RI) detector, and three Ultrastyragel columns (100, 500, and 10^3) connected in series for increasing pore size (eluent: DMF, flow rate: 0.6 mL/min). Wide-angle X-ray diffraction (WAXD) measurement was performed using a Bruker Nanostar U System with incident X-ray wavelength ($\lambda = 0.1542$ nm) operated at room temperature. The collimation system consisted of two cross-coupled Gobel Mirrors and four pinholes. A Histar area detector (Siemens) filled with pressurized xenon gas was used to record the WAXD scattering patterns, with sample to detector distance of 106.1 and 3 cm, respectively. Real-time small angle X-ray scattering (SAXS) measurement was performed at BL01B SWLS beamline in the National Synchrotron Radiation Research Center (NSRRC), Taiwan. The incident X-ray beam was focused vertically by a mirror and monochromated to the energy of 10.5 keV by a germanium (111) double-crystal monochromator. The wavelength (λ) of the X-ray beam was = 1.18095 Å. ^{1}H NMR and ^{13}C NMR spectra were obtained using an INOVA 500 instrument and acetone-d_6 as the solvent. High-resolution solid-state ^{13}C NMR spectroscopy experiment was performed at 25 °C using a Bruker DSX-400 spectrometer operated at a resonance frequency of 100.47 MHz. The experiment was acquired using the cross-polarization (CP)/magic-angle spinning (MAS)/high-power dipolar decoupling (DD) technique. The proton spin-lattice relaxation time in the rotating frame ($T_{1\rho}^H$) was determined via carbon observation using a 90 °C τ-spin lock pulse sequence prior to CP. The acquisition was performed at delay times (τ) ranging from 0.1 to 25 ms with a contact time of 1.0 ms. The PCL-*b*-PVPh/PVP samples were cryo-microtomed at −120 °C for transmission electron microscopic (TEM) observations. Using a Reicher Ultracut microtome was equipped with a Reichert FCS cryochamber and a diamond knife. Staining was accomplished by exposing the samples to the vapor of a 4% aqueous RuO_4 solution for 30 min, resulting in increased contrast because of selectively unstained PCL block.

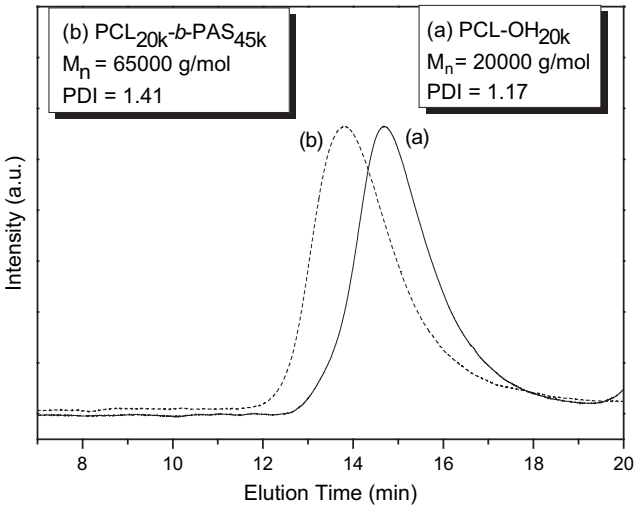

Fig. 1. GPC traces of PCL–OH and PCL-*b*-PAS copolymer.

3. Results and discussion

3.1. Diblock copolymer characterizations

The ring-opening polymerization of ε-caprolactone (ε-CL) initiated by TEMPO-hydroxy benzyl alcohol using $Al(Et)_3$ as a catalyst produced PCL containing one TEMPO chain end. The number average molecular weight of PCL was calculated to be 20,000 g/mol and the polydispersity was less than 1.2. This macroinitiator, PCL-TEMPO, was then employed as the macroinitiator for the TEMPO polymerization with 4-acetoxystyrene (AS) to obtain the PCL-*b*-PAS diblock copolymer. Eventually, all these PCL-*b*-PAS diblock copolymers were converted into PCL-*b*-PVPh diblock copolymers by selective hydrolysis. According to prior literatures [49–51], a number of methods have been employed to convert the 4-acetoxystyrene polymer into corresponding polymer containing phenolic group. It is difficult to proceed the hydrolysis of PAS into PVPh in the presence of PCL because the CL segment is unstable during the hydrolysis process. To overcome this problem, the PAS block of PCL-*b*-PAS was selectively hydrolyzed by reacting with hydrazine hydrate [40].

The GPC trace of the PCL-*b*-PAS block copolymer obtained after living free radical polymerization (TEMPO) is shown in Fig. 1 where the block copolymer prepared from the PCL macroinitiator exhibits a narrow polydispersity and high symmetry of monomodal GPC trace. The absence of the peak corresponding to the PCL macroinitiator confirms the formation of the desired PCL-*b*-PAS diblock copolymer. Complete elimination of the protective groups and the generation of the phenolic hydroxyl groups were confirmed by the ^{1}H NMR spectroscopies as shown in Fig. 2(A). The chemical shift at 2.2 ppm corresponded to the acetyl group of the PCL-*b*-PAS copolymer (in DMSO-d_6) disappears in the spectrum of the hydrolyzed block copolymer and only those polymer backbone protons appear in the chemical shift region from 1 to 2 ppm. In addition, the peak at 8.0 ppm corresponding to the proton of the hydroxyl group appears after the hydrolysis reaction. The FT-IR spectra of PCL-*b*-PAS and PCL-*b*-PVPh shown in Fig. 2(B) indicate that the carbonyl stretching of the PCL-*b*-PAS is split into two bands corresponding to PCL and PAS at 1724 and 1760 cm^{-1}, respectively. The absorption at 1760 cm^{-1} corresponding to the acetyl group of the PCL-*b*-PAS is disappeared and converts to the absorption at 1708 cm^{-1} corresponding to the hydrogen-bonded carbonyl group of PCL after hydrolysis. The broad band at 3350 cm^{-1} in Fig. 2(d) also indicates the occurrence of the hydroxyl groups. The molecular weight of the PCL-*b*-PVPh block copolymer was measured by ^{1}H NMR spectroscopy and GPC [analyzing the relative signal intensities of the protons of PCL (3.6 ppm) and PVPh (6.4–6.8 ppm) segments]. Table 1 lists these calculated molecular weight fractions, the total molecular weights determined by GPC, and polydispersity of these copolymers and homopolymers; the number besiding the descriptor "PCL-*b*-PVPh" represents the molecular weight. Table 2 lists the equilibrium constants previously determined describing the inter-association and all parameters that are required for the calculation according to the Painter–Coleman association model (PCAM) [45] based on Fig. S2. The self-association equilibrium constants, K_2 and K_B, corresponding to the hydroxyl-hydroxyl interaction of PVPh represent the formation of 'dimer' and 'multimer', respectively. For the PVPh-*b*-PCL diblock copolymer, the inter-association equilibrium constant determined through the least square method is ca. 90 which is similar to the PVPh/PCL blend. In addition, the inter-association equilibrium constant K_A of PVPh/PVP (6000) is substantially greater than that of PVPh/PCL (90), implying that the hydroxyl group of PVPh is significantly preferable to interact with the amide carbonyl group of PVP and then interacts with the carbonyl group of PCL.

3.2. Characterizations of diblock copolymer/homopolymer blends

3.2.1. Thermal analyses

Fig. 3 shows the conventional second run DSC thermograms of PVPh-*b*-PCL/PVP blends in various compositions. These two PCL-*b*-PVPh block copolymers possess a single glass transition temperature, suggesting fully miscible of these two blocks. Both glass transition (ca. −60 °C) and melting temperatures (ca. 60 °C) of the PCL appear when the PVP content is 40% or higher. In other words, the higher T_g at ca. 210 ~ 220 °C can be attributed to the T_g of the hydrogen-bonded PVPh/PVP miscible phase, indicating that the effect of molecular weight is unobvious, the lower T_g (ca. −60 °C) is come from the PCL amorphous phase, implying that the PCL dominant phase is excluded when the PVP content is greater than 40 wt% and results in two glass transition temperatures. The micro-phase separation of PCL occurs because the PCL is a significantly weaker hydrogen bond acceptor as compared with PVP. The added PVP preferentially forms hydrogen bonds with PVPh, rather than with PCL, and thus the PCL blocks are excluded from the miscible PVPh/PVP phase. It is worthy to note that T_gs of pure PVPh and pure PVP are both ca. 150 °C, however the T_g of the resultant miscible phase from these two components is significantly higher (ca. 40 ~ 70 °C) due to the strong hydrogen bonding interaction existing between the hydroxyl group of PVPh and the carbonyl group of PVP. In addition, the T_g of the PVPh and PVP mixed phase in PVPh-*b*-PCL/PVP blend (220 °C) is also higher than the corresponding PVPh/PVP homopolymer blend (T_g = 170 ~ 200 °C) [52,53]. In the PVPh-*b*-PMMA/PVP blend system, the PVPh in the block copolymer has less chain ends (one chain end connects to PCL block) than the PVPh homopolymer and thus results in smaller free volume and higher T_g [32].

3.2.2. Solid-state NMR analyses

Solid-state NMR spectroscopy provides further insight into the phase behavior and miscibility of block copolymer/homopolymer blends involving the hydrogen bond interaction. DSC analysis reveals that the domain size of two miscible polymer blend is in a scale ca. 20–40 nm [54]. To further investigate phase domain below 20 nm (ca. 2 ~ 3 nm), the measurement on spin-lattice relaxation time in the rotating frame ($T_{1\rho}^H$) was employed. Fig. 4 shows the ^{13}C CP/MAS spectra of the pure PCL-*b*-PVPh and PCL-*b*-PVPh/PVP blends at various compositions. The peaks at 153 ppm and 177 ppm correspond to the resonances of the phenolic carbon atom of PVPh and the carbonyl carbon of PVP or PCL, respectively. As shown in Fig. 4, the change in the chemical shifts correspond to

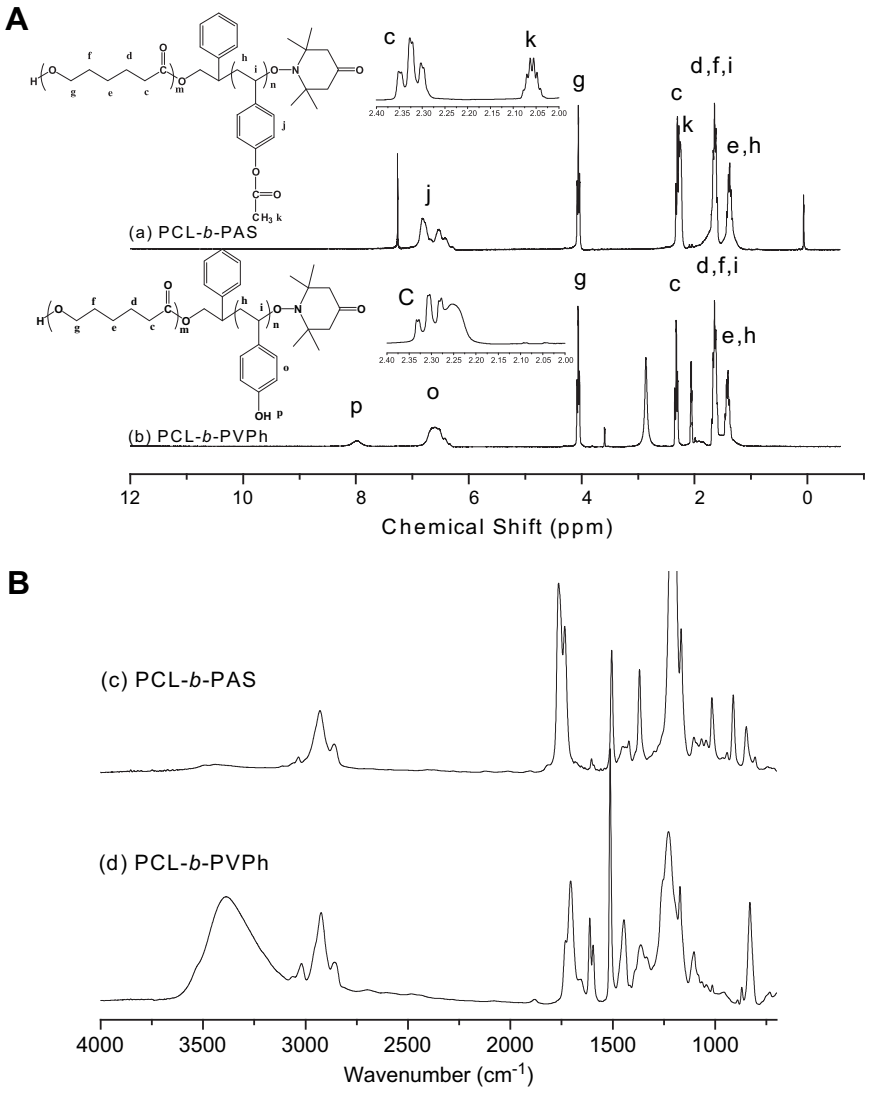

Fig. 2. (A) ^{1}H NMR spectra (a) before hydrolysis, PCL-*b*-PAS, and (b) after hydrolysis, PCL-*b*-PVPh and (B) IR spectra of (c) PCL-*b*-PAS, and (d) PCL-*b*-PVPh ranging from 600 to 4000 cm^{-1}.

phenolic carbon atom in PCL_{20k}-*b*-$PVPh_{45k}$/PVP_{58k} and PCL_{20k}-*b*-$PVPh_{10k}$/PVP_{11k} (50/50) blends are 3 and 4 ppm, respectively, indicating the intermolecular hydrogen bonding interactions between the hydroxyl group of PVPh and the carbonyl group of PVP or PCL segment are present.

The magnetization of resonance is expected to decay according to the following exponential function model $M_\tau = M_0 \exp(-\tau/T_{1\rho}(H))$, where $T_{1\rho}^H$ is the spin-lattice relaxation time in the rotating frame, τ is the delay time used in the experiment, and M_τ is the corresponding resonance. $T_{1\rho}^H$ can be obtained from the slope of the plot of $\ln(M_\tau/M_0)$ vs. τ and results from these blends as shown in Fig. 5. We estimated the homogeneities of these polymer blends through quantitative analyses based on the PCL-*b*-PVPh carbonyl carbon atom's resonance at 177 ppm and the PVPh phenolic carbon atom's resonance at 153 ppm. The PCL-*b*-PVPh exhibits only one $T_{1\rho}^H$, indicating good miscibility and dynamic homogeneity in the pure block copolymer. In contrast, the $T_{1\rho}^H$ decays for the carbonyl and phenolic carbon atoms' resonances of these PCL-*b*-PVPh/PVP blends are not

Table 1
Characterization of PCL-*b*-PVPh copolymers and PVP homopolymer.

Copolymer	M_n[a]	M_w/M_n[b]	T_g (°C)
PCL_{20k}	20,000	1.12	−60
PCL_{68}-*b*-$PVPh_{32}$	31,600	1.32	3
PCL_{50}-*b*-$PVPh_{50}$	42,200	1.28	35
PCL_{40}-*b*-$PVPh_{60}$	49,200	1.37	58
PCL_{30}-*b*-$PVPh_{70}$	65,300	1.41	83
PCL_{28}-*b*-$PVPh_{72}$	69,600	1.42	140
PVP_{58k}	57,800	1.92	150
PVP_{11k}	11,400	1.98	120

[a] Obtained from GPC and ^{1}H NMR measurement.
[b] obtained from GPC analysis.

Table 2
Summary of the self-association and inter-association hydrogen bonding equilibrium constants and thermodynamic parameter of PCL-*b*-PVPh/PVP blends at 25 °C.

Polymer	V	M_w	δ	Equilibrium Constant		
				K_2	K_B	K_A
PVPh	100.0	120.0	10.6	21.0	66.8	–
PCL	107.0	114.0	9.21			90.0
PVP	73.6	115.1	11.0			6000

V: Molar Volume (ml/mol), Mw: Molecular Weight (g/mol), δ: Solubility Parameter (cal/ml)$^{1/2}$, K_2: Dimer self-association equilibrium constant, K_B: Multimer self-association equilibrium constant, K_A: Inter-association equilibrium constant.

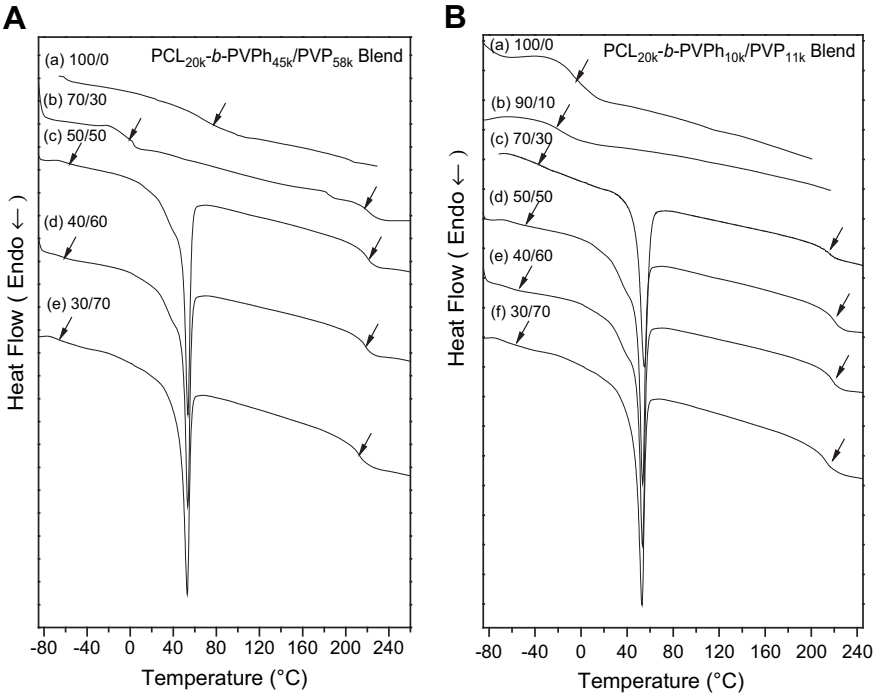

Fig. 3. DSC traces of (A) PCL_{20k}-*b*-$PVPh_{45k}/PVP_{58k}$ and (B) PCL_{20k}-*b*-$PVPh_{10k}/PVP_{11k}$ blends of different compositions.

single-exponential decay. From the slopes of fitting results, values of $T_{1\rho}^{H}$ can be roughly determined and listed in Table 3. More than two domains of these blends were observed based on solid-state NMR analysis, indicating that the phase separation domain was fairly complicated. Further studies on the domain size and the periodicity of the self-assembly structure in PCL-*b*-PVPh/PVP blends were carried out using small angle X-ray scattering and TEM analyses, respectively.

3.2.3. Small angle X-ray scattering

Fig. 6 shows the profiles of Lorentz-corrected intensities of PCL-*b*-PVPh/PVP blends that were annealed at 40 °C for 24 h. The SAXS data provide information concerning the long periods of micro-phase-separated dimensions according to Bragg's law ($d = 2\pi/q^{*}$) where q^{*} is the position of the principal feature. No scattering peak can be observed in pure block copolymers, while scattering peaks at relatively smaller angle are observed with the increase in PVP

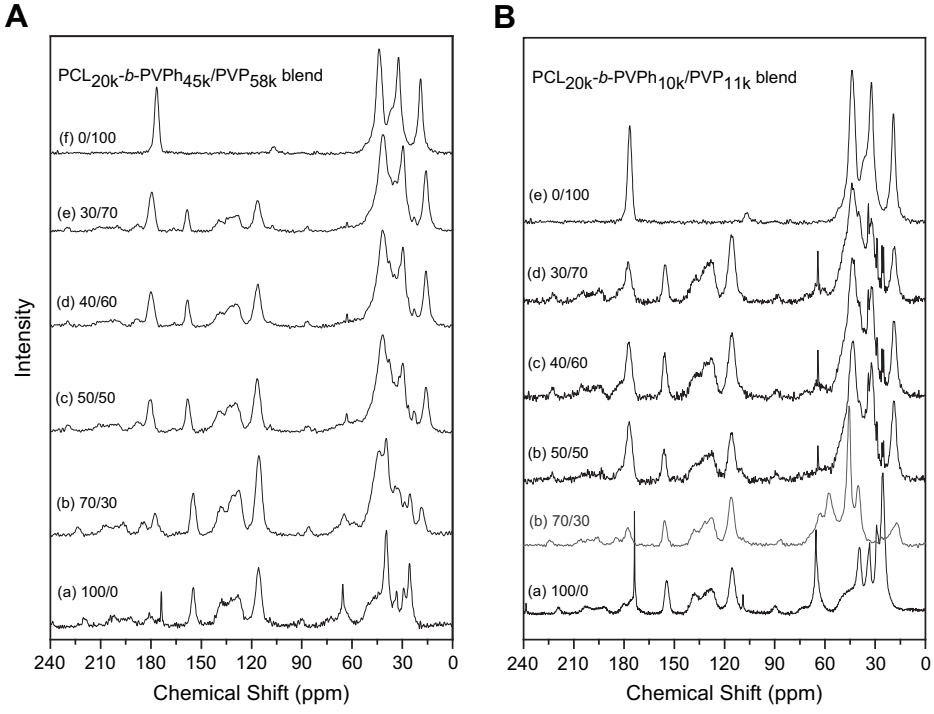

Fig. 4. ^{13}C CP/MAS spectra for (A) PCL_{20k}-*b*-$PVPh_{45k}/PVP_{58k}$ and (B) PCL_{20k}-*b*-$PVPh_{10k}/PVP_{11k}$ blends of different compositions.

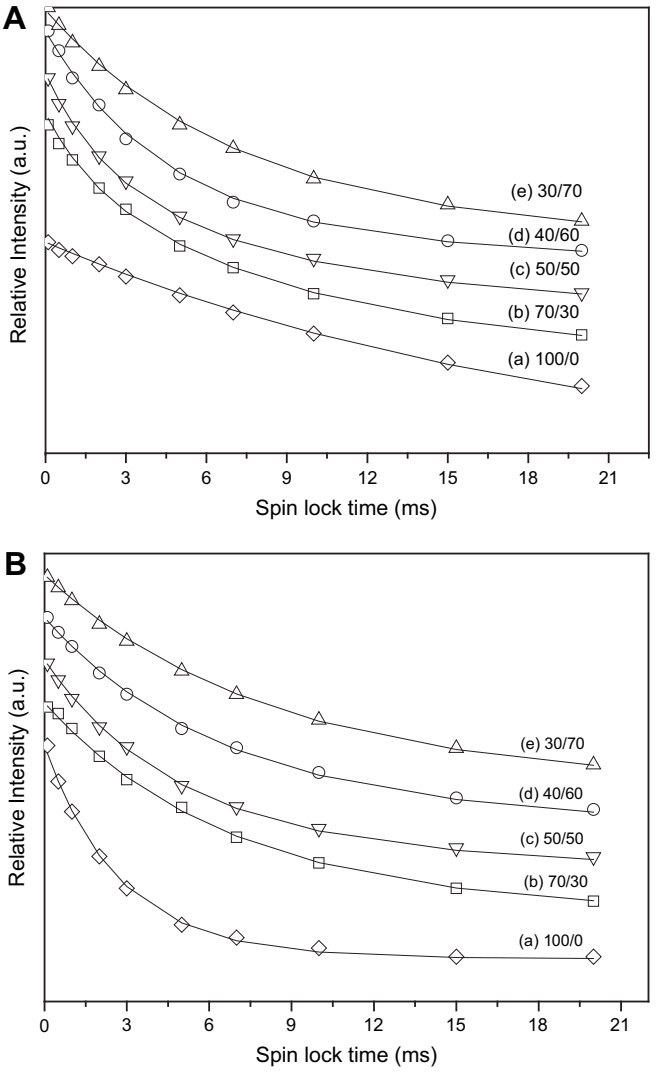

Fig. 5. Solid-state NMR spectroscopic $T_{1\rho}^{H}$ decay curves for PCL_{20k}-*b*-$PVPh_{45k}/PVP_{58k}$ at (A) 177 ppm and (B) 115 ppm with different compositions.

content as shown in Fig. 6(A), indicating that the long period (L) structure increases as a function of the amount of PVP. Rise in long period may stem from the thickening of PCL crystals or the swelling of amorphous layers via incorporation of PVP. The equilibrium degree of chain folding is affected by the transverse dimensions of the flexible amorphous chains. If the molecular weight of the crystalline block remains unchanged while the weight fraction of the amorphous block is increased, these crystalline chains have to fold to accommodate the increase in the transverse dimension of the amorphous chains. The increase in chain folding leads to decrease in the thickness of the crystalline lamellae. Therefore, it is possible to increase the thickness of the amorphous lamellae by decreasing the thickness of the crystalline lamellae.

Table 3
Values of ($T_{1\rho}^{H}$) of various PCL-*b*-PVPh/PVP blend compositions.

PCL_{20k}-b-$PVPh_{45k}/PVP_{58k}$ Blend compositions	($T_{1\rho}^{H}$)	
	177 ppm	153 ppm
100/0	20.4	3.64
70/30	1.54/5.92/10.59	5.84/14.45
50/50	3.93/4.43/12.65	4.44/14.87
40/60	1.94/4.83/10.87	5.64/13.45
30/70	5.27/8.1/10.19	7.44/13.45
PCL_{20k}-b-$PVPh_{10k}/PVP_{11k}$ Blend compositions	($T_{1\rho}^{H}$)	
	177 ppm	153 ppm
100/0	9.82	3.54
70/30	29.21/35.53/44.53	4.48/15.45
50/50	9.21/7.63/15.21	5.84/14.65
40/60	6.64/12.45/16.77	7.64/12.27
30/70	6.17/14.35/19.35	7.94/14.16

The lower molecular weight system of PCL_{20k}-*b*-$PVPh_{10k}/PVP_{11k}$ blends [Fig. 6(B)] exhibits a relatively shaper scattering peaks as compared with the higher molecular weight system PCL_{20k}-*b*-$PVPh_{45k}/PVP_{58k}$ [Fig. 6(A)] due to greater entropy change and the lower molecular weight system results in better miscibility based on thermodynamic reasons. The lower molecular weight system of PCL_{20k}-*b*-$PVPh_{10k}/PVP_{11k}$ blends [Fig. 6(B)] exhibits a relatively shaper scattering peaks as compared with the higher molecular weight system PCL_{20k}-*b*-$PVPh_{45k}/PVP_{58k}$ [Fig. 6(A)] due to greater entropy change and the lower molecular weight system results in better miscibility based on thermodynamic reasons. Therefore, the excluded PCL phase tends to form better regular self-assembly structure. Fig. 6(B) illustrates the presence of a sharper primary peaks and higher-order reflections at q/q^* ratios of 2 and 3 of the PCL_{20k}-*b*-$PVPh_{10k}/PVP_{11k} = 50/50$ blend system, indicating that PCL is arranged as lamellae and its melt morphology is faithfully preserved after crystallization. Couple SAXS peaks located at the positions of $Q_c = 0.01465$ Å^{-1} indicate the presence of a lamellar phase due to the occurrence of the long period of 42.8 nm for PCL_{20k}-*b*-$PVPh_{10k}/PVP_{11k} = 40/60$. As the content of PVP is increased, the higher-order peaks relevant to lamellar morphology become obscured. At 30/70 ratio, the higher-order lamellar peaks are replaced by a broad hump and the lamellar form factor peak is suppressed, implying that the presence of complicated morphology and it may consist of both crystalline lamellae and less perturbed or unperturbed microdomains. The addition of PVP may change the lamellar microdomain structure into a cylinder or finally into a sphere as shown in Fig. 6(a)–(f) (with the ratio of peak positions of $1 : \sqrt{3} : 2$, the presence of hexagonally packed cylinders). The first peak at $Q_c = 0.01422$ Å^{-1} corresponds to an intercylinder distance (L) of 50.9 nm determined from $L = \sqrt{4/3}2\pi/Q_c$. Finally, we also characterized these materials in real space by transmission electron microscopy which can reveal the size and shape within the microdomains.

3.2.4. TEM analyses

The self-assembly morphologies of PCL-*b*-PVPh/PVP blends in bulk state were observed through TEM. The film was stained with RuO_4 where the PVPh chain was deeply stained, the PVP chain was only lightly stained, and the PCL chain was selectively unstained. Fig. 7(A) shows the existence of two phases of the PCL_{20k}-*b*-$PVPh_{10k}/PVP_{11k} = 70/30$ blend possessing a lamellar microstructure observed at room temperature. The gray region corresponds to the mixed phase of the lightly stained PVP and the deeply stained PVPh. The bright region corresponds to a PCL phase that is excluded from the mixed phase because of its relatively weaker ability to form hydrogen bonds with PVPh. Thus, the crystalline PCL is confined within the existing ordered phase due to the vitrification of the amorphous layers. These results are in good agreement with SAXS data for higher-order reflections q/q^* ratios of 2 and 3 with long period ca. 40 ~ 45 nm. Different morphology from PCL_{20k}-*b*-$PVPh_{10k}/PVP_{11k} = 30/70$ was observed as shown in Fig. 7(B), where the micrograph was taken on sections cut perpendicular to the flow direction of the sample, revealing that these cylindrical domains are arranged in a highly ordered hexagonal lattice after melt annealing. This cylindrical nanostructure is formed after annealing at $T_c = 40$ °C, which is consistent with the SAXS data for this composition confirming the cylindrical nanostructure with scattering peaks at q ratio of $1 : \sqrt{3} : 2 : \sqrt{7}$. It can be presumed that the

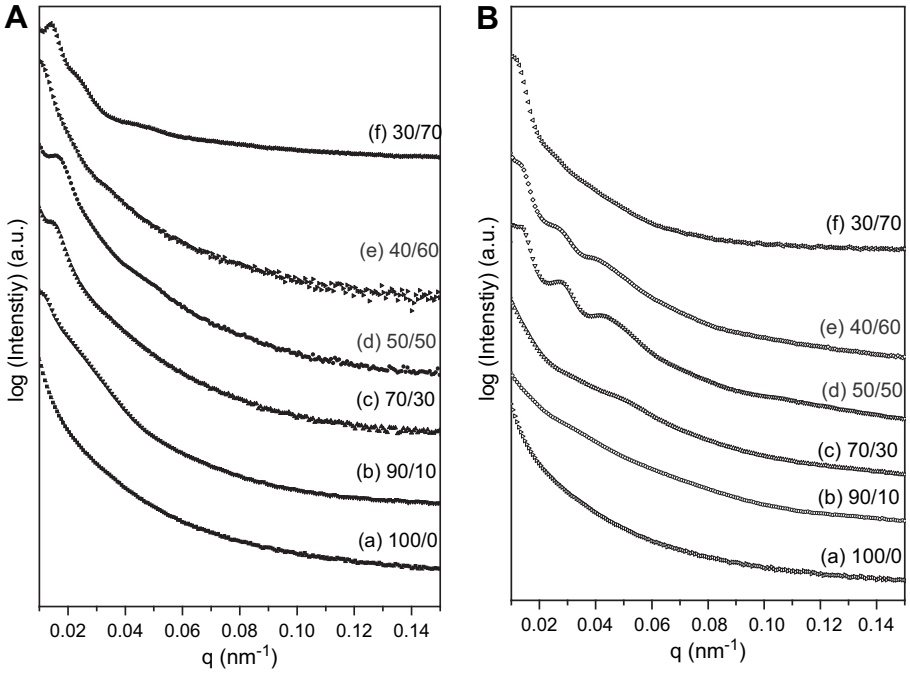

Fig. 6. Profiles of Lorentz-corrected SAXS intensity of (A) PCL_{20k}-*b*-$PVPh_{45k}/PVP_{58k}$ and (B) PCL_{20k}-*b*-$PVPh_{10k}/PVP_{11k}$ blends of different compositions.

high-order diffraction peak is significantly smeared at $\sqrt{7}$, signaling that structure of a significant portion of PCL cylinders is preserved of which intercylinder distance L is ca. 50 nm, close to the SAXS analysis. On the basis of these observations, we can conclude that core shell polygonal cylinders are formed in this case.

3.2.5. Crystallization behavior

Fig. 8 shows DSC cooling curves of PCL-*b*-PVPh/PVP blends obtained at a fixed cooling rate of 5 °C/min. The peak temperature of the crystallization exotherm is defined as freezing temperature (T_f), a relatively higher T_f corresponds to a faster crystallization rate. Clearly, a peculiar crystallization behavior (two exotherms) was found at higher PVP content (lower PCL content), Second exotherm **(II)**, not present in the PCL homopolymer, and appears at much larger undercooling. At lower PCL content, PCL will form a disperse phase as shown in Fig. 7B, whose average size is so small that the number of particles is much greater than the number of active heterogeneities usually present in this polymer. As a result, crystallization takes place with more than one exotherm, and that is precisely termed as "fractionated crystallization" [55,56]. In addition, this copolymer/homopolymer blend shows only one melting temperature in Fig. 3, which is understood by considering that the first crystallization process (exotherm I) is produced by heterogeneous crystallization (continuous domains, in which case crystal growth can propagate throughout the sample) and the second exotherm by homogeneous nucleation (independent (non-connecting) PCL domains in PVPh/PVP mixed phase) as shown in Fig. 7(B). As the PCL content increases (lower PVP content), the nucleation is preferentially heterogeneous as shown in Fig. 8(B). A similar phenomenon has been reported by Chen et al. [57]. They have reported that the strongly-segregated diblock systems display a distinct correlation with the microdomain structure, the T_f decreases abruptly as the melt morphology changed from extended lamellae to dispersed cylinders. An additional drop of T_f is observed as the morphology is further transformed into spheres. The freezing temperature also decreases with the increase of PVP contents in this study. Clearly, the degree of supercooling ($\Delta T = T_m^0 - T_f$, $T_m^0 = 75$ °C) [58] required to initiate crystallization in the lamellar microdomains ($\Delta T = 50$ °C) is comparable to that

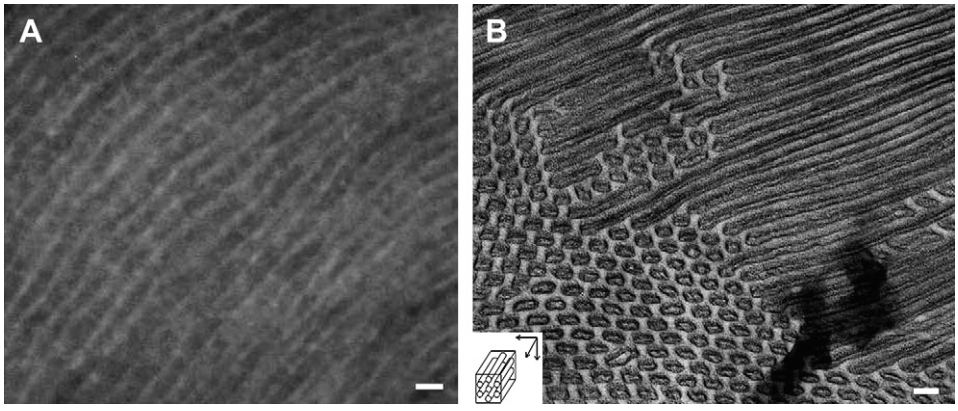

Fig. 7. Transmission electron micrograph of the solution-cast film of the (A) PCL_{20k}-*b*- $PVPh_{10k}/PVP_{11k} = 50/50$ and (B) PCL_{20k}-*b*-$PVPh_{10k}/PVP_{11k} = 30/70$ stained with RuO_4. The dark region (matrix) corresponds to a mixed phase of PVP and PVPh; the white region corresponds to the excluded PCL segment. The scale bar represents 50 nm.

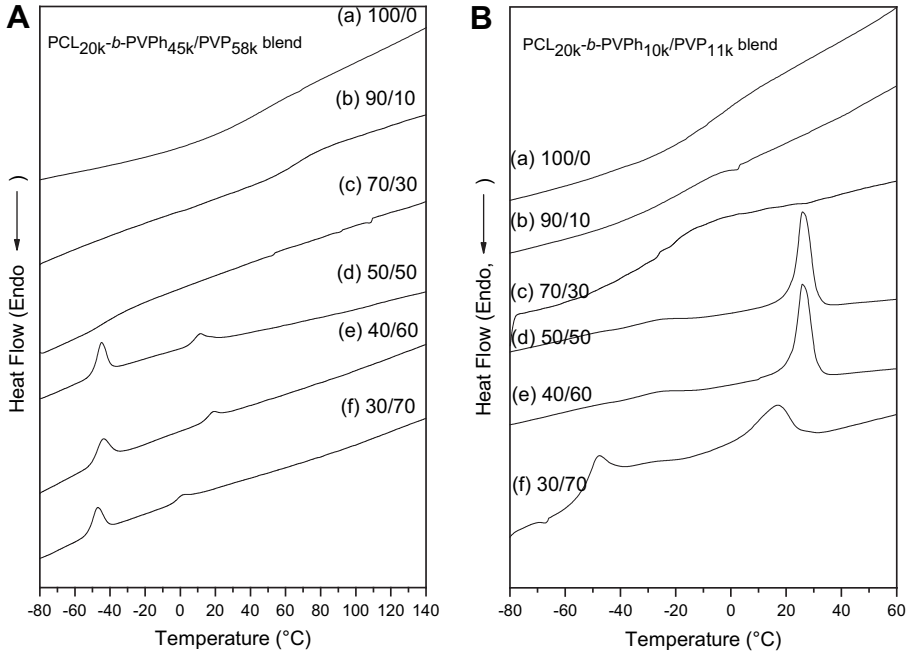

Fig. 8. DSC traces of cooling at 5 °C/min for (A) PCL_{20k}-*b*-$PVPh_{45k}$/PVP_{58k} and (B) PCL_{20k}-*b*-$PVPh_{10k}$/PVP_{11k} blends of different compositions.

associated with the PCL homopolymer ($\Delta T = 42$ °C) while exceedingly faster undercoolings rate is required to initiate the crystallization of cylinder ($\Delta T = 125$ °C). Therefore, the crystallization kinetics exhibits distinct transitions at the compositions with various morphologies, which provides the feasibility of exploiting microdomain pattern by manipulating the crystallization kinetics of the block chains. As shown in Fig. 8A-(f), the PCL-*b*-PVPh/PVP = 30/70 blend shows the main freezing temperature at ca. −50 °C, corresponding to the cylinder structure. As a result, the crystallization behavior of PCL block can be affected because of nanostructure confinement transformation based on small angle X-ray scattering and TEM analyses (from lamellar to cylinder by increasing PVP content) [57].

Further evidence for the exotherm II is come from the homogeneous nucleation at ca. −50 °C, wide-angle X-ray diffraction was employed. The XRD data of PCL-*b*-PVPh/PVP blends are shown in Fig. 9. Two distinct diffraction peaks at $2\theta = 21.5°$ and 23.8° observed correspond to (110) and (200) planes of the orthorhombic crystalline structure of the PCL block [59]. Clearly, only amorphous halo appears in the pure PCL-*b*-PVPh block copolymers because the hydrogen bonding interaction between carbonyl group of PCL and hydroxyl group of PVPh inhibits the PCL crystallization. The intensity of

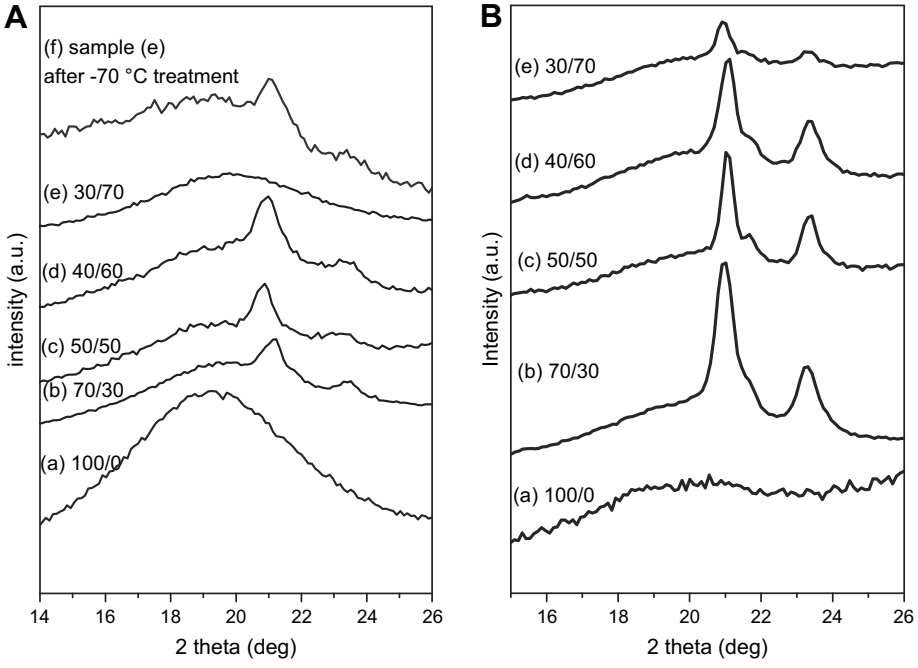

Fig. 9. WAXD patterns of (A) PCL_{20k}-*b*-$PVPh_{45}$k/PVP_{58k} and (B) PCL_{20k}-*b*-$PVPh_{10k}$/PVP_{11k} blends of different compositions.

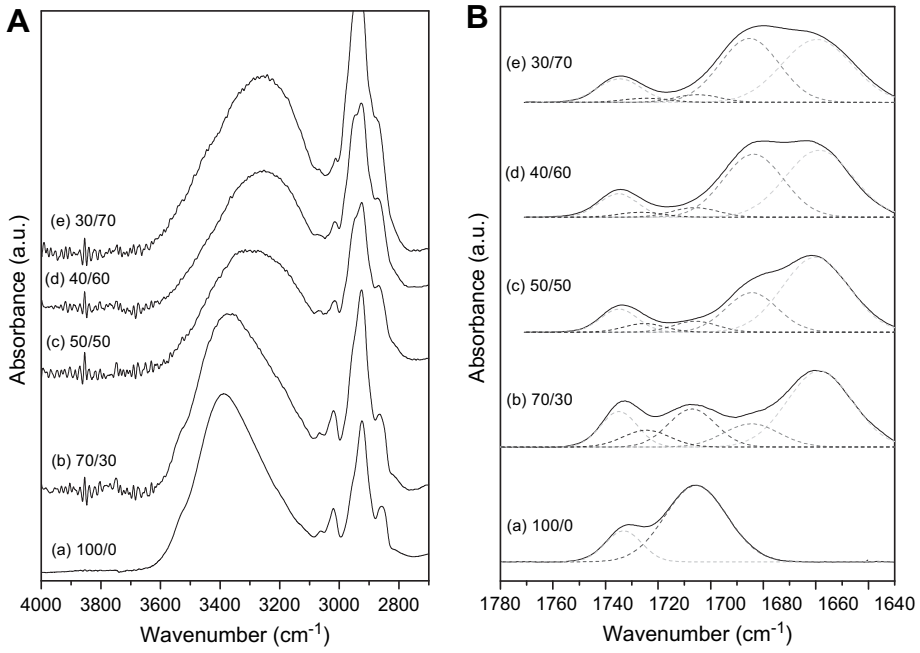

Fig. 10. FT-IR spectra of PCL_{20k}-*b*-$PVPh_{45k}$/PVP_{58k} blends of (A) hydroxyl stretching and (B) carbonyl stretching.

diffraction peak of the crystalline PCL increases with the increase of PVP content (Fig. 9) because the PVP pulls away the PVPh proton donor from the PCL block originally hydrogen-bonded with PVPh block and results in the isolation and crystallization of the PCL block. The degree of crystallinity is significantly decreased with increasing PVP content because the extra PVP is able to interact with PCL block through dipole-dipole interaction. However, the crystal peak disappears as shown in Fig. 9(A)-(e) or significantly decreases in Fig. 9(B)-(e) at higher PVP contents, which is contrast to the DSC analysis as shown in Fig. 3(A)-(e), the PCL-*b*-PVPh/PVP = 30/70 which shows a strong melting transition behavior. In general, the polymer crystallinity measured by XRD is from in-situ measurement and no thermal history is involved in preparing the sample. On the contrary, the polymer crystallinity detected by DSC is correlated with the thermal history because recrystallization may occur during cooling or heating scan. As a result, these samples need to cool down below −50 °C to initiate the crystallization of PCL as shown in Fig. 9(A)-(f). Fig. 9(A)-(f) illustrates that the crystal diffraction peaks of these samples are observed after −70 °C treatment which are also in good agreement with DSC analyses.

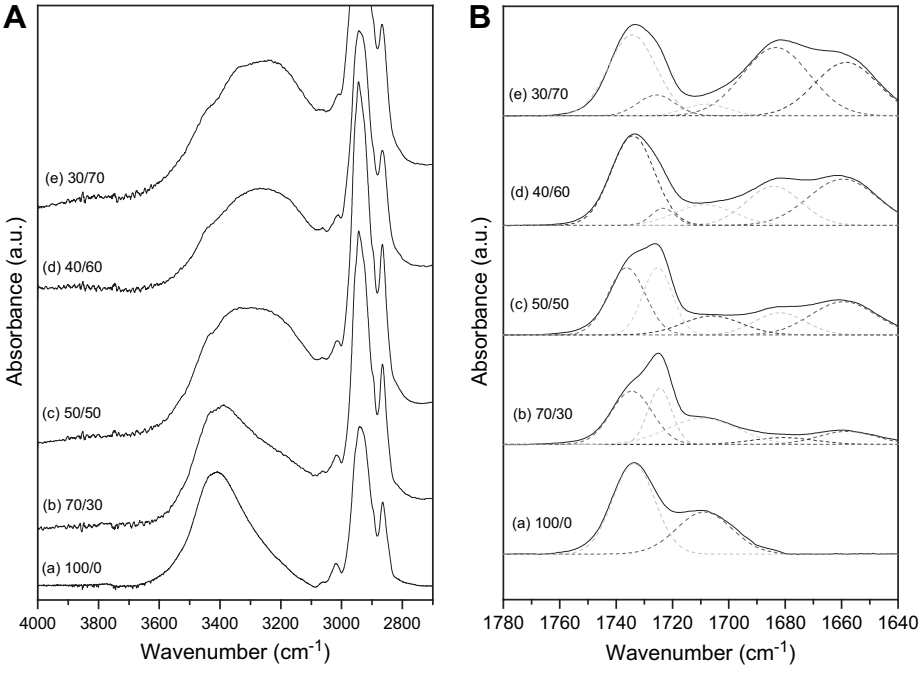

Fig. 11. FT-IR spectra of PCL_{20k}-*b*-$PVPh_{10k}$/PVP_{11k} blends of (A) hydroxyl stretching and (B) carbonyl stretching.

Table 4
Curve-fitting of fraction of hydrogen-bonded carbonyl groups within the PCL-*b*-PVPh/PVP Blends.

PCL_{20k}-*b*-$PVPh_{10k}$/PVP_{58k}	Amorphous C=O			Crystalline C=O			H-bonded C=O			f_b	PVP free C=O			PVP H-bonded C=O			f_b
	υ	$W_{1/2}$	A_f	υ	$W_{1/2}$	A_f	υ	$W_{1/2}$	A_f		υ	$W_{1/2}$	A_f	υ	$W_{1/2}$	A_f	
100/0	1733	19	53				1707	29	47	43.0							
70/30	1735	18	32	1724	11	21	1707	28	30	27.4	1681	20	4	1660	26	13	79.2
50/50	1734	18	27	1724	11	22	1706	28	15	16.9	1681	20	10	1660	27	26	72.1
40/60	1735	18	32	1724	12	9	1706	28	10	12.3	1683	20	17	1660	28	32	67.6
30/70	1735	17	25	1725	11	10	1707	28	7	10.9	1684	22	29	1660	28	29	52.0
PCL_{20k}-*b*-$PVPh_{10k}$/PVP_{11k}	Amorphous C=O			Crystalline C=O			H-bonded C=O			f_b	PVP free C=O			PVP H-bonded C=O			f_b
	υ	$W_{1/2}$	A_f	υ	$W_{1/2}$	A_f	υ	$W_{1/2}$	A_f		υ	$W_{1/2}$	A_f	υ	$W_{1/2}$	A_f	
100/0	1733	17	20				1705	27	80	73.1							
70/30	1734	16	13	1725	12	4	1706	27	23	31.4	1680	20	14	1658	27	46	78.4
50/50	1735	17	10	1725	12	3	1706	27	5	19.4	1683	22	27	1660	28	55	67.1
40/60	1735	16	9	1725	12	3	1706	27	4	17.6	1684	22	37	1660	28	47	56.0
30/70	1735	17	9	1725	12	3	1704	27	3	14.7	1685	22	43	1659	29	42	50.0

3.2.6. FTIR analyses

As mentioned in DSC, solid-state NMR, SAXS, TEM analyses, further evidence is confirmed that the hydrogen bonding strength of PVPh/PVP is greater than the PVPh/PCL. As a result, we will use the FTIR spectroscopies. Figs. 10(A) and 11(A) display FTIR spectra of by PCL_{20k}-*b*-$PVPh_{45k}$/PVP_{58k} and PCL_{20k}-*b*-$PVPh_{10k}$/PVP_{11k} blends in the region from 2700 to 4000 cm^{-1}. The hydroxyl band of the pure PVPh consists of two components, a relatively narrower band at 3525 cm^{-1} corresponding to the free hydroxyl groups and the broad band centered at 3350 cm^{-1} representing a wide distribution of hydrogen-bonded hydroxyl groups. The hydroxyl groups of PVPh interact with carbonyl groups of PVP more preferentially at lower than with carbonyl groups of PCL in the PCL-*b*-PVPh copolymer. The intensity of the hydrogen-bonded hydroxyl groups appearing at 3250 cm^{-1} increase gradually with the increase of PVP content in the blend as would be expected. At lower PVP content in the blend and higher PVPh content in the copolymer, the excessive hydroxyl groups in PVPh have the opportunity to associate with the PCL blocks (i.e., the signal of the hydrogen-bonded hydroxyl groups broadens). The frequency difference ($\Delta\nu$) between the hydrogen-bonded hydroxyl and the free hydroxyl can be used to roughly estimate the average the hydrogen bonding strength [60]. In this respect, the hydrogen bonding interaction between PVPh hydroxyl and PVP carbonyl ($\Delta\nu = 275\ cm^{-1}$) is significantly stronger than that between PVPh hydroxyl and PCL carbonyl ($\Delta\nu = 95\ cm^{-1}$) in these blends, which is consistent with relative values of the inter-association equilibrium constant, where the K_A of PVPh/PVP (6000) is substantially greater than that of PVPh/PCL (90).

Figs. 10(B) and 11(B) present FT-IR spectra ranging from 1630 to 1780 cm^{-1} of PCL_{20k}-*b*-$PVPh_{45k}$/PVP_{58k} and PCL_{20k}-*b*-$PVPh_{10k}$/PVP_{11k} blends, corresponding to carbonyl stretching region, respectively. The PCL-*b*-PVPh/PVP blend possesses five carbonyl stretching signals, including free carbonyl of PVP (1680 cm^{-1}), H-bonded carbonyl of PVP (1660 cm^{-1}), free, H-bonded, and crystalline carbonyl stretching bands of PCL centered at 1730 cm^{-1}, 1708 cm^{-1} and 1724 cm^{-1}, respectively. When the PVP content in the blend is increased, the H-bonded carbonyl of PVP appears at 1660 cm^{-1}, reflecting the presence of intermolecular hydrogen bonding interaction between the PVP and PVPh units, revealing that interaction between PVPh hydroxyl and PVP carbonyl is dominant in these blends, the PCL blocks are thus excluded from the PVPh/PVP amorphous phase. Therefore, it is reasonable to assign the band at 1724 cm^{-1} as the PCL crystalline conformation [as shown in Fig. 7 (B)-(b) PCL-b-PVPh/PVP = 70/30]. Table 4 summarizes these curve-fitting results obtained from FT-IR spectra, indicating that the hydroxyl–carbonyl inter-association between PVPh and PCL decreases gradually with the increase of PVP content in these blends. The smaller molecular weights in the PVPh block in diblock copolymer and PVP homopolymer contains a greater fraction of the hydrogen-bonded carbonyl that may come from loss of internal degrees of rotational freedom and resulted in better miscibility based on thermodynamic reasons. As a result, the PCL segment is excluded from the miscible blend between PVPh segment of the diblock copolymer and PVP to form its own domains and thus PCL crystallizes, which is consistent with DSC, SAXS, XRD, and TEM analyses.

4. Conclusions

In this study, specific interaction, morphologies and phase behaviors mediated by hydrogen bonding interactions of A-B/C type blends have been studied. First, the PCL-*b*-PVPh copolymer has been successfully synthesized by the combination of ring-opening polymerization and living free radical polymerization. DSC, FTIR, TEM, solid-state NMR, and SAXS techniques have been employed to investigate in detail the miscibility, phase behavior and hydrogen bonding interaction mechanism of this novel A-B/C type polymer blending system composed of miscible PVPh-*b*-PCL and PVP. FTIR, XRD, and DSC measurements provide evidence that PVP is a significantly stronger hydrogen bond acceptor than the PCL with PVPh. ^{13}C CP/MAS solid-state NMR spectra indicate the occurrence of the micro-phase separation in these blends. TEM micrographs and SAXS data indicate that the change in compositions of the PVPh-*b*-PCL/PVP blends induces changes in the micro-phase separation structures through the mediation of hydrogen bonding interactions. The final phase behavior and morphology vary with the increase of PVP content because of the competition between PVP/PVPh and PCL/PVP units. Based on thermodynamic reason of miscibility, the smaller molecular weight in the PVPh block in diblock copolymer and the PVP homopolymer contains a greater fraction of the hydrogen-bonded carbonyl amide group of PVP, cause indirectly the high degree of phase separation among these blends.

Acknowledgment

This work was supported financially by the National Science Council of the R.O.C. under Contract No. NSC 97-2221-E-110-013-MY3 and NSC 97-2120-M-009-003 and Ministry of Education "Aim for the top University" (MOEATU) program. The SAXS experiments were conducted at beamline BL17B3 at the National Synchrotron Radiation Research Center (NSRRC), Taiwan.

Appendix. Supplementary data

Supplementary data associated with this article can be found in the online version, at doi:10.1016/j.polymer.2009.09.012.

References

[1] Hashimoto T, Tanaka H, Hasegawa H. Macromolecules 1990;23:4378.
[2] Bendejacq D, Ponsinet V, Joanicot M. Macromolecules 2002;35:6645.
[3] Holoubek J, Baldrian J, Lednicky F, Malkova S, Lal J. Macromol Chem Phys 2006;207:1834.
[4] Tucker PS, Barlow JW, Paul DR. Macromolecules 1988;21:2794.
[5] Tucker PS, Paul DR. Macromolecules 1988;21:2801.
[6] Lowenhaupt B, Steurer A, Hellmann GP, Gallot Y. Macromolecules 1994;27:908.
[7] Han YK, Pearce EM, Kwei TK. Macromolecules 2000;33:1321.
[8] Zhao JQ, Pearce EM, Kwei TK. Macromolecules 1997;30:7119.
[9] Jiang M, Xie HK. Prog Polym Sci 1991;16:977.
[10] Kosonen H, Ruokolainen J, Nyholm P, Ikkala O. Macromolecules 2001;34:3046.
[11] Matsushita Y. Macromolecules 2007;40:771.
[12] Lee JH, Balsara NP, Chakraborty AK, Krishnamoorti R, Hammouda B. Macromolecules 2002;35:7748.
[13] Akaba M, Nojima S. Polym J 2006;38:559.
[14] Gao JP, Wei Y, Li B, Han YC. Polymer 2008;49:2354.
[15] Huang YY, Chen HL, Hashimoto T. Macromolecules 2003;36:764.
[16] Likhman AE, Semenov AN. Macromolecules 1997;30:7273.
[17] Huang YY, Hsu JY, Chen HL, Hashimoto T. Macromolecules 2007;40:3700.
[18] Chen WC, Kuo SW, Lu CH, Chang FC. Macromolecules 2009;42:3580.
[19] Stoykvich MP, Edwards EW, Solak HH. Phys Rev Lett 2006;97:147802.
[20] Jinnai H, Hasegawa H, Nishikawa Y, Sevink GJA, Braunfeld MB, Agard DA, et al. Macromol Rapid Commun 2006;27:1424.
[21] Kuo SW. Polym Int 2009;58:455.
[22] Tu CW, Kuo SW, Chang FC. Polymer 2009;50:2958.
[23] Huang P, Zhu L, Cheng SZD, Ge Q, Quirk RP, Thomas EL, et al. Macromolecules 2001;34:6649.
[24] Vavasour JD, Whitmore MD. Macromolecules 2001;34:3471.
[25] Hameed N, Guo Q. Polymer 2008;49:922.
[26] Hameed N, Guo Q. Polymer 2008;49:5268.
[27] Chen D, Jiang M. Acc Chem Res 2005;38:494.
[28] Coleman MM, Painter PC. Prog Polym Sci 1995;20:1.
[29] Manestrel CL, Bhagwagar DE, Painter PC, Coleman MM, Graf JF. Macromolecules 1992;25:7101.
[30] Jo WH, Kwon YK, Kwon IH. Macromolecules 1991;24:4708.
[31] Kuo SW, Lin CL, Chang FC. Macromolecules 2002;35:278.
[32] Chen WC, Kuo SW, Jeng US, Chang FC. Macromolecules 2008;41:1401.
[33] Lee HF, Kuo SW, Huang CF, Lu JS, Chan SC, Chang FC. Macromolecules 2006;39:5458.
[34] Chen HL, Hsiao SC, Lin TL, Yanauchi K, Hasegawa H, Hashimoto T. Macromolecules 2001;34:671.
[35] Eastmond GC. Adv Polym Sci 1999;149:223.
[36] Kuo SW, Chan SC, Chang FC. Macromolecules 2003;36:6653.
[37] Kuo SW, Chan SC, Wu HD, Chang FC. Macromolecules 2005;38:4729.
[38] Kuo SW, Chan SC, Chang FC. J Polym Sci, Polym Phys 2004;42:117.
[39] Kuo SW, Huang CF, Chang FC. J Polym Sci, Polym Phys 2001;39:1348.
[40] Kuo SW, Huang CF, Lu CH, Chang FC. Macromol Chem Phys 2006;207:2006.
[41] Chen SC, Kuo SW, Liao CS, Chang FC. Macromolecules 2008;41:8865.
[42] Lin CL, Chen WC, Kuo SW, Chang FC. Polymer 2006;47:3436.
[43] Kuo SW, Liu WP, Chang FC. Macromol Chem Phys 2005;206:2307.
[44] Lin CL, Chen WC, Liao CS, Su YC, Huang CF, Kuo SW, et al. Macromolecules 2005;38:6435.
[45] Coleman MM, Graf JF, Painter PC. Specific interactions and the miscibility of polymer blends. Lancaster, PA: Technomic Publishing; 1991.
[46] Hu Y, Motzer HR, Etxeberria AM, Fernadez-Berridi MJ, Iruin JJ, Painter PC, et al. Macromol Chem Phys 2000;201:705.
[47] Noda I, Ozaki Y. In: Two-dimensional correlation spectroscopy. John Wiley& Sons; 2004.
[48] Noda I. J Am Chem Soc 1989;111:8116.
[49] Kuo SW, Chang FC. Macromolecules 2001;34:7737.
[50] Kuo SW, Xu H, Huang CF, Chang FC. J Polym Sci, Polym Phys 2002;40:2313.
[51] Kuo SW, Liu WP, Chang FC. Macromolecules 2003;36:5168.
[52] Kuo SW, Chang FC. Macromolecules 2001;34:5224.
[53] Prinos A, Pompros A, Panayiotou C. Polymer 1998;14:3011.
[54] Kuo SW, Chang FC. Macromolecules 2001;34:4089.
[55] Balsamo V, von Gyldenfeldt F, Stadler R. Macromolecules 1999;32:1226.
[56] Balsamo V, von Gyldenfeldt F, Stadler R. Macromol Chem Phys 1996;197:3317.
[57] Hsu JY, Hsieh IF, Nandan B, Chiu FC, Chen JH, Jeng US, et al. Macromolecules 2007;40:5014.
[58] Kuo SW, Chang FC. Macromol Chem Phys 2001;202:3112.
[59] Sun J, Chen X, He C, Jing X. Macromolecules 2006;39:3717.
[60] Moskala EJ, Varnell DF, Coleman MM. Polymer 1985;26:228.